Radiative Heat Feedback in Aluminized Hybrid Fuel Combustion

D. Pastrone, L. Galfetti**, G. Colombo**, and L.T. DeLuca***
** Dipartimento di Energetica, Politecnico di Torino, I-10129 Turin, Italy*
*** SPLab, Dipartimento di Energetica, Politecnico di Milano, I-20156 Milan, Italy*

Abstract
An experimental and theoretical investigation was performed to investigate the radiant energy emitted by aluminized HTPB hybrid solid fuels burned in a gaseous 50% O_2, 50% N_2 mixture. The radiant energy was measured by means of a micro-calorimeter for different fuel compositions, including nano-aluminized fuels and HTPB/paraffin-based fuels. A one-dimensional model has been developed to describe the combustion, flow, and radiant transport processes by aluminum and alumina particles near the surface of a burning aluminized propellant. The equations of mass and momentum have been solved to obtain velocity profiles. A proper temperature profile and aluminium burning correlation have been assumed. The decoupled radiative transfer equation has also been solved using the two-flux model to obtain the radiant flux profiles and the radiative heat feedback to the propellant surface.

1. Introduction

Metallized hybrid fuels have been studied for a long time, both theoretically and experimentally[1]. Aluminum seems, for many reasons, the best metal to be used. Aluminized fuels are extremely attractive due to the high heat of reaction, aluminum high density and radiative heat feedback coming back to the grain which may improve the hybrid fuels low regression rate. Anyway, due to the fact that aluminum addition changes several properties of the flame and of the solid grain, it is not so clear if the aluminium presence can always enhance the burn rate. In order to improve the knowledge of the involved phenomena, an experimental and numerical investigation is performed into the radiant transport processes by aluminum and alumina particles near the surface of the solid fuel grain in hybrid fuel combustion.
The experimental part of this work aims to investigate the thermal radiation effects in hybrid combustion. In 1991, Estey et al.[2] showed that thermal radiation improved correlations for metal-loaded solid fuels whereas for non metallized hydrocarbon fuels convective heat transfer correlations were able to give better results. Strand et al.[3], in 1994, in contrast to Estey's results, found that radiation from soot greatly affected the pure HTPB regression rate, giving also the suggestion to investigate the thermal radiation effects with the oxidizer/fuel ratio and combustion chamber pressure. This is only one example to show that questions still exists about the extent of radiant heat flux in hybrid motors, especially considering modern solid hybrid fuels.
Due to the fact that the objective of the present work is not combustion efficiency but radiative heat feedback, a realistic yet relatively simple model has been developed on the basis of previous works[4-6]. Brewster and Parry,[4] used a one-dimensional two-flux model, which takes into account droplet burn rate and two-phase flow while disregarding two-dimensional flow considerations and Al droplet size distribution, to evaluate radiative heat feedback in aluminized composite solid propellants. This approach is here adapted to hybrid propellant combustion and coupled with the classical modelization for combustion in the turbulent boundary layer[5-7].

2. Experimental set-up

The solid fuel grain samples used were rectangular (15 x 22 x 4 mm) to allow combustion in a turbulent boundary layer with heat and mass transfer. Samples were arranged in a rectangular cross section chamber (32 x 24 mm, 100 mm long); lateral windows allowed to visualize the combustion process (Figure 1, Figure 2 and Figure 5). The fuel sample was ignited using a hot wire; the pressure was kept constant during the test due to an automatic pressure control system. A high-speed and high resolution video-camera was used, in order to investigate the flame structure, metal particle aggregation and combustion, ignition and flame development over the fuel surface. The radiant energy,

emitted during the combustion process, was measured by means of a micro-calorimeter, put on the top of the chamber. Details of the experimental set-up are shown in Figures 1 and 2, and a sketch of the lay-out in Figure 3.

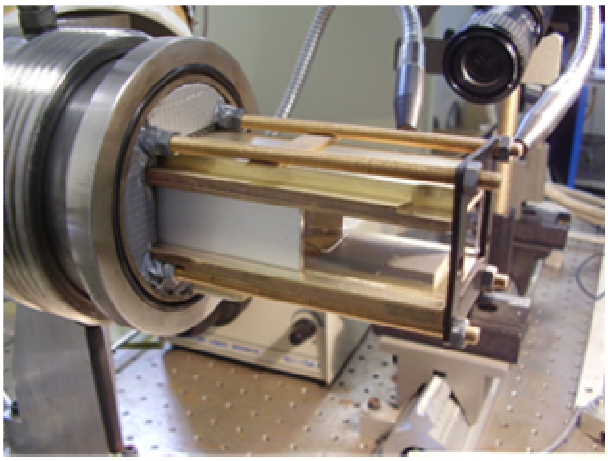

Figure 1 : Detailed view of the combustion chamber

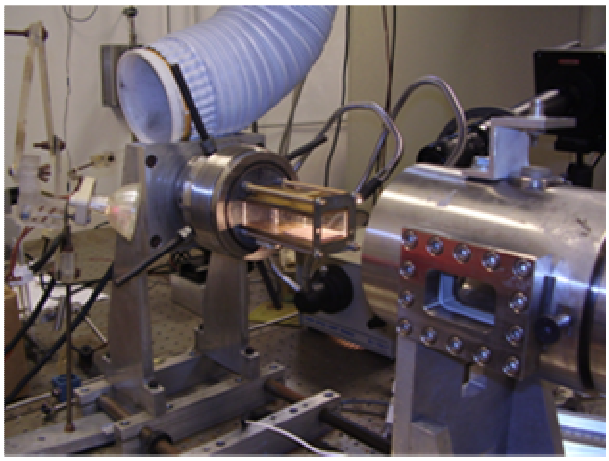

Figure 2 : View of the experimental set-up

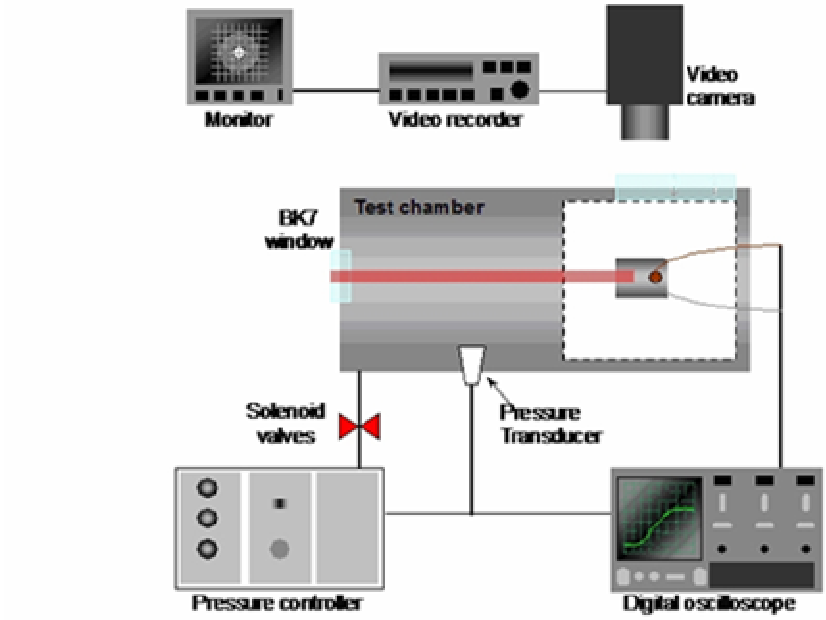

Figure 3 : Schematic view of the experimental set-up

3. Radiant energy measurement

The radiant energy flux sensor used in this work is a "home made" improved version of Zenin's micro-calorimeter. The sensor is manufactured and calibrated at SPLab. The sensitive element consists in a thin copper disk (0.3 mm) with a Copper-Constantan thermocouple welded on the back surface (Figure 4). The front surface of the disk is exposed to the radiant flux and is blackened with a black paint to increase the absorbivity of the sensitive element. The calorimeter thickness is small enough to have a low thermal inertia, allowing dynamic radiant flux measurements over most of the burning time of the hybrid solid fuel samples. The calorimeter temperature rise is sufficiently small to make radiation energy losses negligible as compared to the measured heat flux. This is essential to ensure a good accuracy because radiant losses are not taken into account in the sensor model.

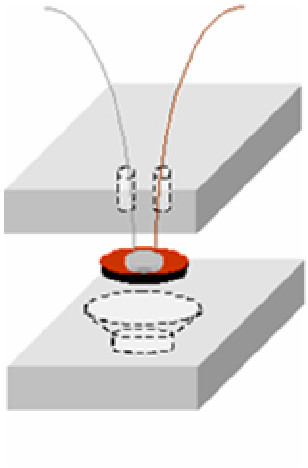

Figure 4 : Calorimeter sensitive element assembled

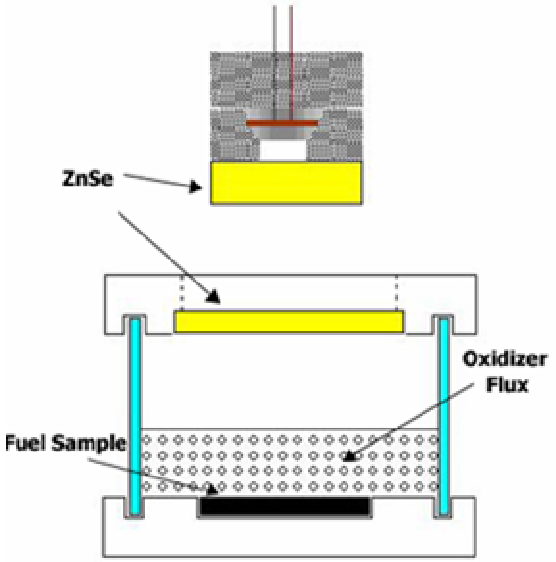

Figure 5 : Schematic front view of the test chamber

To avoid heating or cooling of the calorimeter, due to convective and conductive energy exchange, the copper disk has to be thermally insulated. This is obtained by placing the copper disk in a thick plexiglas housing, with its blackened surface facing a cylindrical ZnSe window. The window allows most of the radiation to pass through, heating up the disk, but prevents the combustion gases from reaching the calorimeter. Conduction through the plexiglas housing, in which the calorimeter is perfectly sealed, is negligible, because the disk just leans onto the conical hole (Figure 4). Therefore, the contact surface is minimal; moreover, the plexiglas housing thermal inertia is such that the housing does not heat up significantly during the sample burning.

The housing back plate has two 1 mm drilled holes to allow the thermocouple wires to get through it and be connected to the compensated wires on the test chamber. The calorimeter is separated from the housing by a very thin layer (about 1 mm) of air (Figure 6), therefore, energy transmission from the disk to the plexiglas housing is mainly conductive. Calibration results show that losses are in general small.

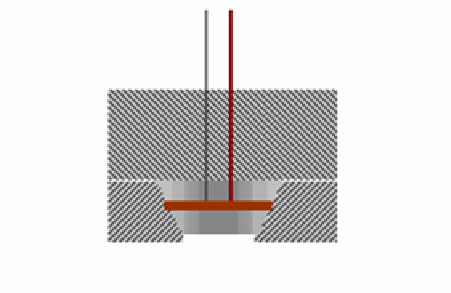

Figure 6 : Lateral sensor view

4. Sensor Model and Calibration

The sensor mathematical model is based on the energy balance equation, where the energy losses are taken into account by a convective loss term. Assuming a constant convection coefficient, the rate of the calorimeter energy increase, is given by:

$$m\ c\ dT(t) / dt = q_m(t)\ A\ \alpha - \Delta T(t)\ h_m\ A_m \quad (1)$$

where T(t) is the calorimeter temperature, $q_m(t)$ is the radiant heat flux impinging on the calorimeter, α is the fraction of radiant heat flux which is not absorbed or reflected by the window, $\Delta T(t) = T(t)-T_1$ is the difference between calorimeter and ambient temperature, m is the calorimeter mass, c is the calorimeter specific heat, h_m is an average convection coefficient, A_m is the area involved in the thermal exchange, and A is the window area. From Eq. (1), two characteristic parameters can be defined:

$$K = \alpha /(h_m A_m) \text{ and } \tau = m\ c /(h_m A_m)$$

which are respectively the sensitivity factor, and the temperature time constant.
From the model equation (1) the radiant heat flux impinging on the calorimeter, $q_m(t)$, is the sum of the calorimeter energy increase rate (the first term in Eq. 2) and the heat loss term (the second term in Eq. 2):

$$q_m(t) = (\tau/K)\ (1/A)\ dT(t) / dt\ +\ (1/A)\ \Delta T(t) / K \quad (2)$$

Therefore, the radiant flux can be measured easily from the micro-calorimeter temperature by means of Eq. 2, once K and τ are known. The data reduction procedure is as follows: the digitized thermocouple signal is converted into temperature; temperature and its derivative are substituted in Eq. 2, along with the sensor parameters (measured from the calibration), obtaining the instantaneous radiant flux $q_m(t)$.
For each sensor, K and τ are experimentally derived by means of a proper calibration procedure. The sensor is exposed to a known radiant power step function, q (from a laser beam), and its response is recorded and optimally fitted to the ideal model temperature step response (3), obtained from Eq. 1.

$$T(t) = A\ K\ q(1 - \exp(t/\ \tau)) + T \quad (3)$$

Calibration is performed at four radiant levels: 20, 40, 60 and 80 W . The calibration procedure allows to compute K and τ, minimizing the square error between experimental and model response. Each parameter is calculated averaging the values obtained in five tests at each radiant level; parameters are scattered: $\sigma(\tau/K) = 8.1$ %; $\sigma(K) = 77$ %, confirming the need to calibrate each sensor. Calibration results are summarized in Table 1.

Table 1 : Micro-calorimeter typical calibration results

Laser beam power [W]	Laser beam power impinging on the calorimeter sensitive element [W]	τ / K	1 / K
20	4.25	0.0491	0.0188
40	9.40	0.0505	0.0187
60	15.05	0.0566	0.0311
80	20.45	0.0561	0.0188

5. Radiant energy measurements results

The radiant energy flux is measured for fuel samples formulations ranging from non-metallized (fuel no. 1 and no. 5, respectively pure HTPB and HTPB + paraffin-based), to a mildly metallized (Al 5%, fuels no. 2 and 3) to a heavily metallized (Al 15%, fuel no. 4). See Table 2 for the detailed compositions investigated.

Table 2 : Fuel compositions investigated in this study

Fuel No.	Fuel Type	Al type	Al mass %	Al nominal grain size [µm]
1	Pure HTPB[a]	---	---	---
2	HTPB + Al	Al_01a	5 %	0.17
3	HTPB + Al	Al_05	5 %	30
4	HTPB + Al	Al_06	15 %	50
5	HTPB + paraffin	---	0 %	---

[a] Hydroxyl Terminated PolyButadiene R 45

Tests were performed using a gaseous 50% O_2 and 50% N_2 mixture, at p = 7 bar. The temperature detected by the micro-calorimeter is shown in Figure 7. A comparison among the radiant energy emitted during the combustion of the investigated fuels shows that the lowest contribution is that of the HTPB+paraffin fuel, whereas the highest is that of mildly metallized fuels. No significant differences can be appreciated in the comparison between micro (30 µm) and nano (0.17 µm) powders. The trend of pure HTPB and HTPB enriched with coarse Al particles is in between these curves.

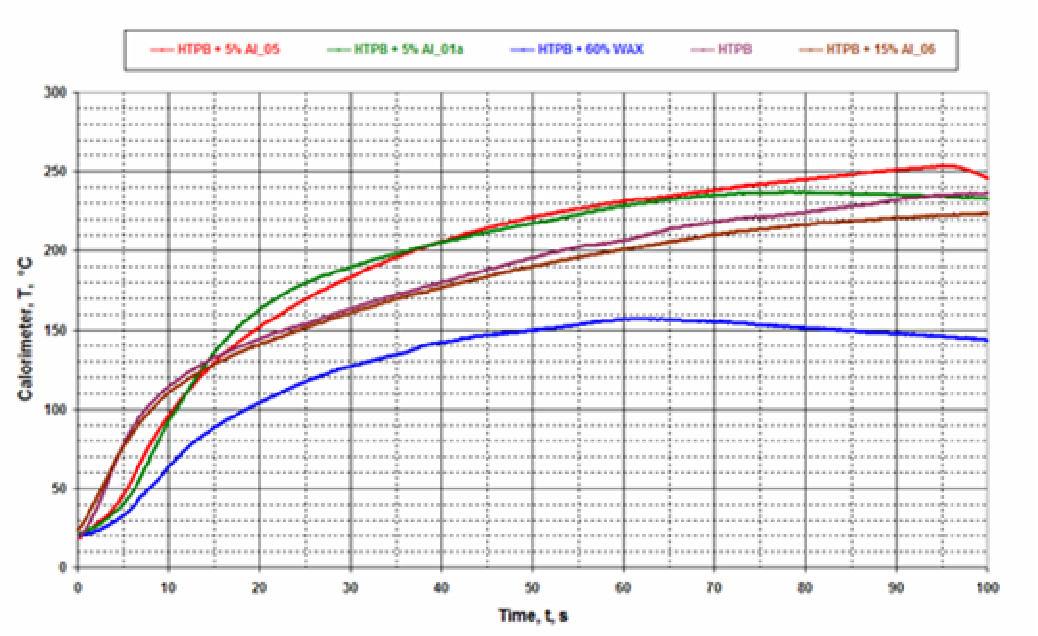

Figure 7 : Temperature measured by the calorimeter during the combustion of Table 1 solid fuels

Radiant energy fluxes are shown in Fig. 8. The larger reactivity of nano and micro Al spherical powders, in comparison with that of bigger (50 μm, flaked) particles, is responsible for the larger radiant energy fluxes. Fuels 1 and 4 give approximately the same radiant flux because large Al particles do not react in the small chamber of the experimental set-up. Responsible for radiation in this case is mainly soot, originated by HTPB pyrolysis, and chemical species in the gaseous combustion products, such as CO_2, H_2O and CO. A lower amount of soot during the combustion of fuel 5, related to lower HTPB content, explains the significantly lower radiant energy emission. Radiant fluxes, after the ignition transient, are estimated to be in the range 1.0 – 2.0 W/cm^2. A comparison between the combustion process of a hybrid fuel and a solid propellant is shown in Figure 9; these two frames, taken from a high speed video recording of the combustion processes in these two different situations, performed under the same operating conditions, can give a visual explanation of the low measured radiant energy.

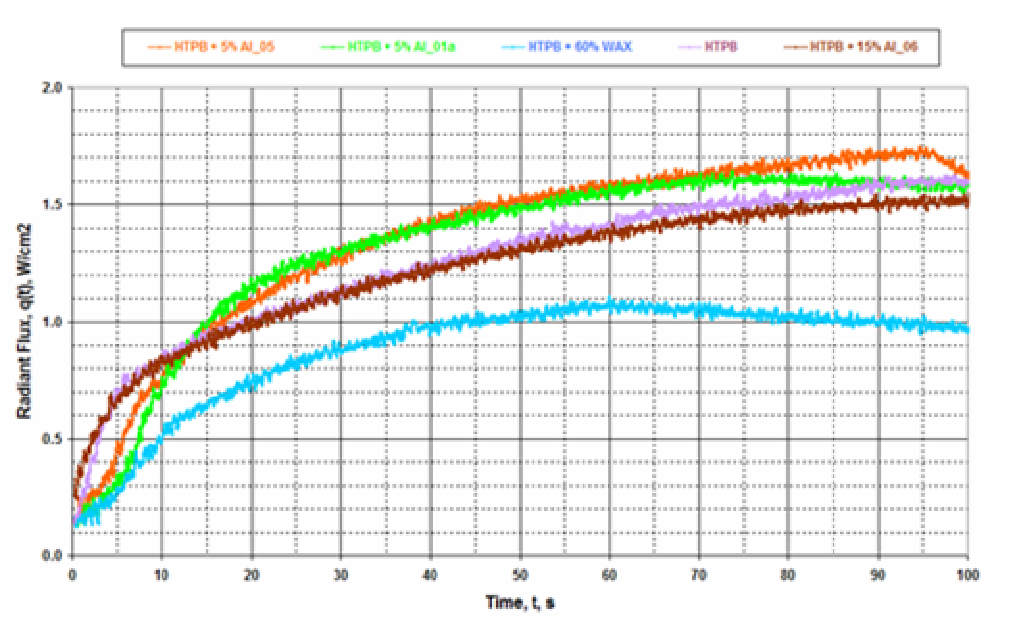

Figure 8 : Measured radiant flux vs. time during combustion of solid fuels presented in Table 1

Figure 9 : Comparison between the combustion process of a hybrid fuel (HTPB + 15% Al_05) and a solid propellant (HTPB + 14% Al_05, AP-based). Pressure, Al grain size and video recording conditions are the same in the two situations.

5. Numerical model

Two set of equations are used: the first set is related to combustion and flowfield, while the second describes the radiation. This two sets of equations can be decoupled, assuming that radiation has negligible effects on energy transport and flame height.

5.1 Combustion - Flow model

The present model encompasses the region of space adjacent to the surface of the fuel grain. The origin of the x coordinate is at the leading edge of the grain, while the origin of the y coordinate is at the surface of the grain which is stationary: the propellant is assumed to move upward at the linear regression rate r. The computational field is splitted into three regions. Region 1 is the inner region from the solid fuel grain surface up to the flame, region 2 is the zone where the aluminum combustion occurs and region 3 is the region above the combustion zone. Combustion of the gaseous fuel due to HTPB pyrolysis is supposed to be very fast, and a laminar flame model is assumed, while a distributed Al droplet combustion is taken into account. In all the three regions, a two-phase flow is considered (the word phase is here used to indicate species having the same fluid dynamic and thermodynamic properties). In the inner region, one phase consists of the aluminum droplets while the second phase is a gas mixture considered to have the properties of the most abundant pyrolysis product of HTPB: 1,3 butadiene gas[9]. In region 2 the first phase consists of the burning aluminium droplets, while the other phase consists of combustion gases plus oxidizer and Al_2O_3 particles. These oxide particles and gas are assumed to be in thermal equilibrium at temperature T_g and to have the same velocity U_g. Gas properties such as molecular mass, heat capacity, viscosity and conductivity, are assumed to be constant in each region. The flame height is evaluated following the analysis presented in Ref. 4: the model assumes a given regression rate (supposed to be experimentally measured) and disregards radiation effects. The unknowns are the aluminum particle velocity U_{al}, gas velocity U_g , gas temperature T_g, aluminum particle diameter D_{al} and species volume fractions. The aluminium combustion is evaluated assuming the burning law[10]:

$$D_{al} = \left(D_{0,al}{}^{1.8} - Kt\right)^{\frac{1}{1.8}} \qquad \text{where} \qquad K = \frac{(C_{O2} + 0.6C_{H2O} + 0.22C_{CO2})p^{0.1}T_{al}^{0.2}}{1.468x10^{6}} \tag{4}$$

where the pressure p is measured in bar, the droplet temperature T_{al} in Kelvin, the diameter D_{al} in meters and the time t in seconds. It is supposed that the initial aluminum temperature T_{al} and mass fractions of O_2, H_2O and CO_2 assume the values computed[11] at the given pressure and flame local mixture ratio. The alumina mass production rate per unit volume can be consequently computed evaluating the aluminum consumption rate $\dot{m}_{al}'''$:

$$\dot{m}_{al}''' = -1.667\frac{\rho_{al} f_{al} K}{D_{al}} = \frac{d(\rho_{al} f_{al} U_{al})}{dy} \tag{5}$$

The momentum equation for the two-phase flow and the gas equation:

$$\begin{cases} \rho_{al} U_{al}\dfrac{dU_{al}}{dy} = 3\rho_g (U_g - U_{al})\left|U_g - U_{al}\right| C_d / 4D_{al} \\ \rho_g U_g f_g \dfrac{dU_g}{dy} = -3\rho_g f_{al}(U_g - U_{al})\left|U_g - U_{al}\right|\dfrac{C_d}{4D_{al}} - \dfrac{dp}{dx} \\ \dfrac{dp}{p} = \dfrac{dR}{R} + \dfrac{dT_g}{T_g} + \dfrac{d\rho_g}{\rho_g} \end{cases} \tag{6}$$

Finally, instead of using the energy equation, a proper temperature profile can be assumed. Ancillary equations are used to evaluate the aluminum volume fraction f_{al} and gas phase (including alumina particles in region 2 and 3) volume fraction f_g, while the drag coefficient C_d is approximated assuming a value of $24/Re_D$. A boundary value problem arises, which is solved by a procedure which is based on Newton's method.[12]

5.2 Radiation model

Once the combustion-flow model is solved, thermodynamic and flowfield properties are obtained. These properties can be used to evaluate the forward (I^+) and backward (I^-) radiant intensity, integrating the governing equations of the two-flux radiation model[4]:

$$\begin{cases} \dfrac{dI^+}{dy} = -(a+s)I^+ + s\,I^- + k_{al}I_b(T_s) + k_{ox}I_b(T_{ox}) \\ -\dfrac{dI^-}{dy} = -(a+s)I^- + s\,I^+ + k_{al}I_b(T_s) + k_{ox}I_b(T_{ox}) \end{cases} \tag{7}$$

The two-flux absorption coefficient a and scattering coefficient s (sum of the contributes coming from aluminum droplets, possibly including flame envelope, and aluminum oxides particles) and the emissivity coefficients k are :

$$\begin{aligned} a &= a_{al} + a_{ox} \\ s &= s_{al} + s_{ox} \\ \\ a_i &= 3fv_i\alpha_i / D_i \qquad \text{i = al, ox} \\ s_i &= 3fv_i\rho_i B_i / D_i \\ k_i &= 3fv_i\varepsilon_i / D_i \end{aligned} \tag{8}$$

and $I_b(T)$ is the blackbody radiant intensity at the given temperature T_s (aluminum droplet surface) or T_{ox} (aluminum oxide particle). Note that the not burning aluminum droplet and the aluminum oxide particle are assumed to be in thermal equilibrium with the gas ($T=T_g$), while, following Ref. 4, the burning aluminum droplet is assumed to have T = 2320 K. Under the combustion zone (region 1), only aluminum droplets are present, while, above the combustion zone (region 3) aluminum is burned and only aluminum oxide particles are present. The optical constant, shown in Table 3, are taken from Ref. 4.

Table 3: Parameters used in the radiation model

	absorptivity α	reflectivity ρ	emissivity ε	backscattering B
Al droplet	0.1	0.9	0.1 if not burning 1.0 if burning	0.5
Al_2O_3 particle	0.45	0.55	0.45	0.3

Reflection and emission by the propellant is assumed to be negligible. At the grain surface the forward radiation intensity is zero: $(I^+)_{y=0} = 0$, while the backward radiation intensity is an unknown of primary interest. Again a boundary value problem arises and a boundary condition is needed. Brewster and Parry[4] suggest $dI^+/dx\ (x \rightarrow \infty) = 0$.

5.3 Numerical results

Results are presented, considering the test of fuel No. 4. The assumed temperature profile is shown in Figure 11. It is obtained considering a grain surface temperature of 800 K, a wall temperature (y = 40 mm) of 300 K, a flame temperature of 2400 K (it is assumed that the hybrid combustion occurs at a mixture ratio which is a half of the stoichiometric value) and assuming that $d^2T/dy^2 = 400\ dT/dy$. Figure 11 also shows aluminum particle diameter. The mechanism of aluminum agglomeration is not addressed here and the aluminum particle diameter is assumed to be 50 μm. The effective aluminum oxide particle size is assumed to be 5 μm. Oxidant mass flow is evaluated to be about 132 kg/(m^2s) and a regression rate of 1 mm/s is considered. Dynamic viscosity is evaluated[11] at flame condition (0.77 10-4 Pa s), and considered to be constant. Figure 12 shows the aluminum and gas phase velocity, while the radiant fluxes ($q = \pi I$) are shown in Figure 13, considering $dI^+/dy = 0$ for y = 40 mm.

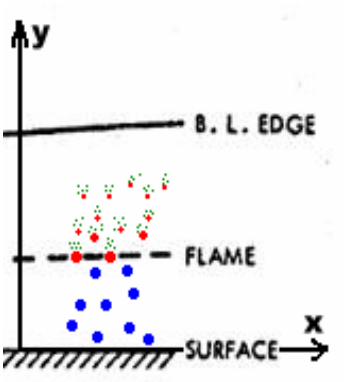

Figure 10 : Schematic

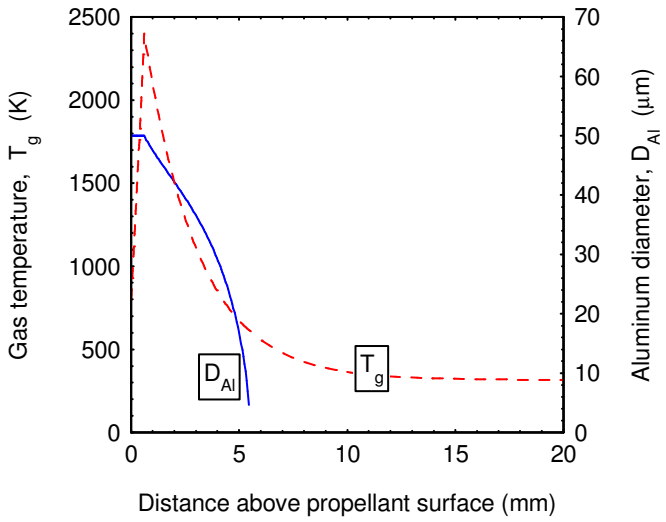

Figure 11 : Aluminum diameter and assumed gas temperature

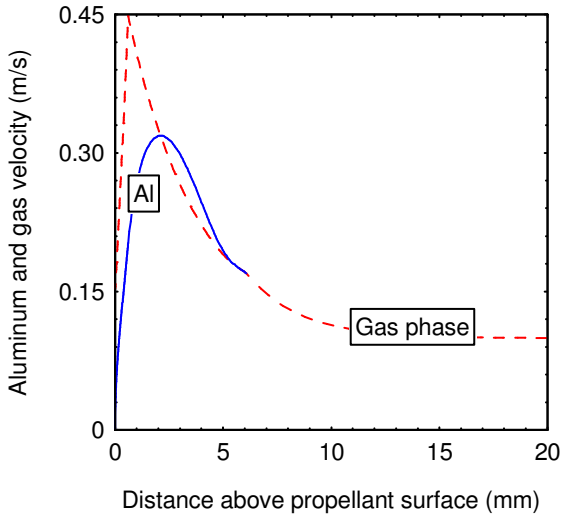

Figure 12 : Aluminum and gas phase velocity

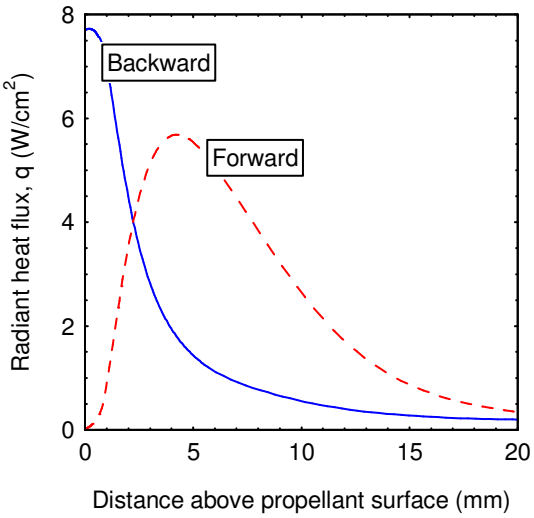

Figure 13 : Forward and backward radiant heat flux

5. Conclusions

Radiant energy emitted during the combustion process of metallized solid hybrid fuels was measured for different compositions. Under the investigated operating conditions the energy flux, measured on the opposite side of the solid fuel regression rate, was very low, of the order of 1–2 W/cm^2; the influence of aluminum particles and soot, generated by HTPB pyrolysis, was shown. The developed mathematical model, under reasonable assumptions, confirmed the experimental trend. Future work will be directed to measure flame temperature and position, wall temperature, Al oxide diameter and radiant energy impinging on the fuel surface.

References

[1] Smoot, L.D. and Price, C.F., "Regression Rates of Metallized Hybrid Fuel Systems", *AIAA Journal*, Vol. 4 , No. 5, pp. 910-915, 1965.

[2] Estey, P.N., Altman, D. and McFarlane, J.S., "An Evaluation of Scaling Effects for Hybrid Rocket Motors", AIAA Paper 91-2517, June 1991.

[3] Strand, L.D., Jones, M.D., Ray, R.L. and Cohen, N.S., "Characterization of Hybrid rocket Internal Heat Flux and HTPB Fuel Pyrolysis", AIAA Paper 94-2876, June 1994.

[4] Brewster, M.Q. and Parry, D.L., "Radiative Heat Feedback in Aluminized Solid Propellant Combustion.", *Journal of Thermophysics and Heat Transfer*, Vol. 2, No. 2, pp. 123-130, 1988.

[5] Marxman, G.A. and Gilbert, M., "Turbulent Boundary Layer Combustion in the Hybrid Rocket", Ninth International Symposium on Combustion, The Combustion Institute, pp. 371-383, 1963.

[6] Marxman, G.A., Wooldridge, C.E. and Muzzy, R.J., "Fundamentals of Hybrid Boundary-Layer Combustion", Progress in Aeronautics and Astronautics, Vol. 15, pp. 485-522, 1964.

[7] Marxman, G.A., "Combustion in the turbulent boundary layer on a vaporizing surface", Tenth International Symposium on Combustion, The Combustion Institute, pp.1337-1349, 1965.

[8] Ishihara, A., Brewster, M.Q., Sheridan, T.A. and Krier, H., "The Influence of Radiative Heat Feedback on Burning Rate in Aluminized Propellants", *Combustion and Flame,* 84: 141-153, 1991.

[9] Chiaverini, M.J., Kuo, K.K., Peretz, A. and Harting, G.C., "Regression-Rate and Heat-Transfer Correlations for Hybrid Rocket Combustion", *Journal of Propulsion and Power*, Vol. 17, No. 1, pp. 99-110, 2001.

[10] Beckstead, M.W., "Correlating Aluminum Burning Times", *Combustion, Explosion, and Shock Waves*, Vol. 41, No. 5, pp.533-546, 2005.

[11] McBride, B.J., Reno, M.A. and Gordon, S., "CET 93, Chemical Equilibrium with Thermal Transport Properties": an interim version of the Nasa Lewis complex chemical equilibria with applications, 1993.

[12] Colasurdo, G., Pastrone, D., "Indirect Optimization Method for Impulsive Transfer," Paper AIAA 94-3762, Aug. 1994.

This page has been purposedly left blank